Planar Meanderline Ferrite-Dielectric Phase Shifter

E. R. BERTIL HANSSON, SHEEL ADITYA, MEMBER, IEEE, AND MATS A. LARSSON

Abstract—**This paper presents the design of meanderline circuits with multilayer ferrite-dielectric embedding. New expressions are developed for the even- and the odd-mode admittances for an infinite meanderline in such a structure. It is shown that the effective dielectric constants and the effective relative permeabilities for some of the multilayer structures are simply related. An efficient synthesis routine for the design of meanderline circuits is described. Effect of different parameters on the phase shift has been studied experimentally. It is indicated that the present structure can result in a compact phase shifter with an improved figure of merit, peak power-handling capability, and temperature stability.**

I. Introduction

FERRITE phase shifters based on meander-folded lines have been known for several years. In 1966, Jones described the design of a stripline phase shifter [1] by using the theories of Bolljahn and Matthaei [2]. A couple of years later, Roome and Hair [3] gave a first-order theory for the functioning of reciprocal as well as nonreciprocal phase shifters using microstrip techniques. In separating the meanderline from the ferrite by a thin dielectric sheet, the peak power capability was shown to increase [4]; also the total losses and the differential phase shift were found to decrease. However, by choosing a proper combination of materials and geometry, a net improvement of the figure of merit was achieved [5]. Thus experimental results indicate that optimal performance of the meanderline phase shifter demands a multilayer structure. Accordingly, the multilayer ferrite-dielectric structure shown in Fig. 1(a) has been investigated for its application in meanderline phase shifters.

II. Design of an Infinite Meanderline Embedded in a Multilayer Ferrite-Dielectric Structure

For a meanderline surrounded by layers of different media, Weiss [6] showed, under the quasi-TEM approximation, that the dispersion law and the image admittance for the forward-wave propagation are given by

$$\tan^2\frac{\Phi}{4}=\frac{Y_e(\Phi)}{Y_o(\Phi)}\tan\{k_e(\Phi)A/2\}\tan\{k_o(\Phi)A/2\} \quad (1)$$

$$Y_{\text{im}}(\Phi)=\sqrt{Y_e(\Phi)Y_o(\Phi)\frac{\tan\{k_e(\Phi)A/2\}}{\tan\{k_o(\Phi)A/2\}}} \quad (2)$$

where

$$k_i^2(\Phi)=\frac{\omega^2}{C^2}\epsilon_{\text{eff}\,i}(\Phi)\mu_{\text{eff}\,i}(\Phi), \qquad i=e,o. \quad (3)$$

In these equations, Φ is the phase increment per unit cell of the periodic meanderline structure and Y_e and Y_o are the even- and the odd-mode admittances corresponding to the two normal modes assumed to propagate on an array of infinitely long strips. The dimensional parameter A is the length of the meanderlines which are obtained by connecting alternate strips (Fig. 1(b)). For an even mode, the phase difference between adjacent strips is $\Phi/2$, and for an odd mode, it is $\Phi/2+\pi$, or $(\Phi+2\pi)/2$ [6]. For the special case of $\Phi=0$, the phase difference per unit cell for the even and the odd mode is 0 and 2π, respectively.

Appearance of Φ following a parameter is meant to emphasize the fact that the parameter changes with Φ. For

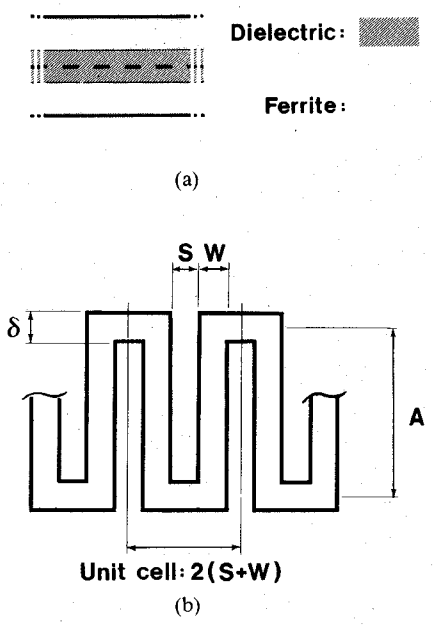

Fig. 1. (a) Meanderline embedded in a ferrite-dielectric composite. (b) Meanderline pattern showing the unit cell and other dimensions of the meanderline.

Manuscript received September 30, 1980; revised October 13, 1980. A condensed version of this paper has been presented at the 1980 IEEE-MTTS International Microwave Symposium, Washington, DC. This work was supported in part by the Swedish Board for Technical Development. A full length version is found in the internal report [15].

E. R. B. Hansson was with the Division of Network Theory, Chalmers University of Technology, Gothenburg, Sweden. He is now with Microwave Development Laboratories, Inc., Natick, MA, 01760.

S. Aditya was with the Division of Network Theory, Chalmers University of Technology, Gothenburg, Sweden, under a collaboration program supported by Swedish International Development Agency. He is now with the Department of Electrical Engineering, Indian Institute of Technology, Delhi, India.

M. A. Larsson is with the Division of Network Theory, Chalmers University of Technology, Gothenburg, Sweden.

0018-9480/81/0300-0209$00.75 ©1981 IEEE

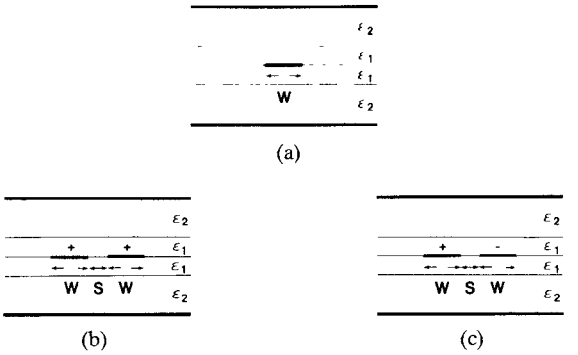

Fig. 2. Basic four-layer structures involving two dielectrics. (a) Single line. (b) Double line with even excitation. (c) Double line with odd excitation.

meanderline phase shifter structures reported previously [7], maximum differential phase shift was obtained for $\Phi = 180°$. In the present case of an inhomogeneous construction where the dielectric layers are placed between the ferrite and the meanderline, it is found that a higher value of Φ needs to be used to achieve the same result.

To obtain the characteristics of an infinite meanderline embedded in a multilayer ferrite-dielectric structure, an approach different from that of Weiss [6] is adopted here. The present approach involves the following steps.

A. Characteristics of a Single Line and Two Coupled Lines

The characteristics of the single line and the double line in the four-layer dielectric–dielectric structure, shown in Fig. 2, are worked out by the method of Lennartsson [8]. In this method, the lines are described in terms of filling factors α_s, α_{de}, and α_{do} and characteristic admittances Y_{sv}, Y_{dev}, and Y_{dov}, the latter for the lines in vacuum. The indices *s*, *de*, and *do* indicate, respectively, the parameters corresponding to the single line and the even- and the odd-mode excitation of the double line.

B. Algorithm for Efficient Analysis

By considering the linewidth W as a variable and the other parameters of the structure as constants we can expand each one of the six characterizing parameters in a power series in W, thereby approximating the actual behavior over a limited linewidth interval. If the structure is analyzed for N different values of $W, W_1 \cdots W_N$, one can fit polynomial approximations of the order $N-1$ to the obtained parameter values resulting in the following equation system:

$$[W_a][C]=[S] \tag{4}$$

where

$$[W_a]=\begin{bmatrix} W_1^0 & W_1^1 & \cdots & W_1^{N-1} \\ W_2^0 & W_2^1 & \cdots & W_2^{N-1} \\ \vdots & \vdots & & \vdots \\ W_N^0 & W_N^1 & & W_N^{N-1} \end{bmatrix}.$$

$[C]$ is a coefficient matrix and $[S]$ is the matrix formed by the N analysis result vectors.

By solving (4) for the coefficient matrix $[C]$ one gets

$$[C]=[W_a]^{-1}[S]. \tag{5}$$

Using $[C]$, the structure can be analyzed for an arbitrary linewidth W in the interval according to

$$[R]=[W_b][C] \tag{6}$$

where

$$[W_b]=[W^0 W^1 \cdots W^{N-1}]$$

and

$$[R]=[\alpha_e(W) \quad \alpha_o(W) \quad \alpha_s(W) \quad Y_{vde}(W) \cdot Y_{vdo}(W) \quad Y_{vs}(W)].$$

Based on the coefficient matrix $[C]$ and (6), the analysis can be performed several orders of magnitude faster than by direct use of, for instance, a finite difference method [8].

C. Characteristics of an Infinite Meanderline

Leblond *et al.* [9] derived, for the admittance of an infinite coupled line, an expression which, under the present definition of Φ, is written as

$$Y(\Phi)=2y_{oo}+4\sum_{n=1}^{\infty} y_{on}\sin^2(n\Phi/4) \tag{7}$$

in which y_{on} are the mututal admittances to the ground (y_{oo}) and to the neighboring conductors ($y_{on}, n\neq 0$), respectively. For $\Phi=0$ and $\Phi=2\pi$, (7) simplifies considerably. Since these values of Φ correspond to the even- and the odd-mode excitation, respectively, for the special case of zero phase increment per unit cell, one can write

$$Y(0)=Y_e \tag{8}$$

$$Y(2\pi)=Y_o. \tag{9}$$

Thus from (7)

$$Y_e=2y_{oo} \tag{10}$$

$$Y_o=2y_{oo}+4\sum_{n=1}^{\infty} y_{on}, \qquad \text{where } n \text{ takes on odd values.} \tag{11}$$

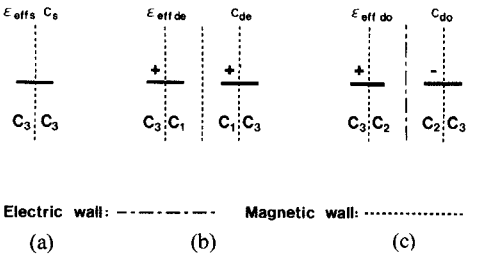

Fig. 3. Schematic representation of single- and double-line configurations, with associated capacitances and effective dielectric constants. (a) Single line. (b) Double line with even excitation. (c) Double line with odd excitation.

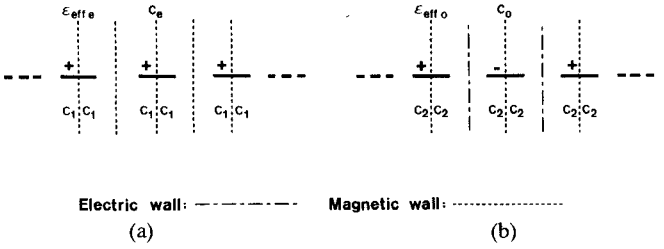

Fig. 4. Schematic representation of infinite coupled line configuration, with associated capacitances and effective dielectric constants. (a) Even excitation. (b) Odd excitation.

Next, retaining only the first two terms in (7), i.e., neglecting the coupling between nonadjacent strips, one obtains

$$Y(\Phi) = Y_e + (Y_o - Y_e)\sin^2(\Phi/4). \tag{12}$$

Consider the single- and the double-line configurations represented by Fig. 3(a), (b), and (c), with the associated capacitances C_s, C_{de}, and C_{do}, and the effective dielectric constants $\epsilon_{\text{eff}\,s}$, $\epsilon_{\text{eff}\,de}$, and $\epsilon_{\text{eff}\,do}$. The corresponding infinite coupled line case is represented by Fig. 4(a) and (b), with C_e and C_o as the associated capacitances and $\epsilon_{\text{eff}\,e}$ and $\epsilon_{\text{eff}\,o}$ as the associated effective dielectric constants. In Figs. 3 and 4, electric and magnetic walls are centered between the lines. Also, magnetic walls are assumed to pass through the middle of the lines. These assumptions involve a first-order approximation for the cases of Fig. 3(b) and (c). From Figs. 3 and 4

$$C_e = 2C_1 = 2C_{de} - C_s \tag{13}$$

$$C_o = 2C_2 = 2C_{do} - C_s. \tag{14}$$

In the following, subscript i is used in place of both e and o. For the vacuum case

$$C_{iv} = 2C_{div} - C_{sv}, \qquad i = e, o. \tag{15}$$

Recognizing that

$$Y_{div} = c_o C_{div} \tag{16}$$

$$Y_{sv} = c_o C_{sv} \tag{17}$$

where c_o is the speed of light in vacuum, from (15)

$$Y_{iv} = 2Y_{div} - Y_{sv}. \tag{18}$$

Defining

$$\epsilon_{\text{eff}\,i} = C_i / C_{iv} \tag{19}$$

$$\epsilon_{\text{eff}\,di} = C_{di} / C_{div} \tag{20}$$

$$\epsilon_{\text{eff}\,s} = C_s / C_{sv} \tag{21}$$

one gets

$$\epsilon_{\text{eff}\,i} = (2\epsilon_{\text{eff}\,di} Y_{div} - \epsilon_{\text{eff}\,s} Y_{sv})/(2Y_{div} - Y_{sv}). \tag{22}$$

Also, using

$$Y_i / Y_{iv} = (\epsilon_{\text{eff}\,i})^{1/2} \tag{23}$$

one obtains

$$Y_i = \{(2\epsilon_{\text{eff}\,di} Y_{div} - \epsilon_{\text{eff}\,s} Y_{sv})(2Y_{div} - Y_{sv})\}^{1/2}. \tag{24}$$

Substitution of (18) and (24) in (12) yields $Y_{iv}(\Phi)$ and $Y_i(\Phi)$, respectively. Thus for instance

$$Y_e(\Phi) = Y(\Phi) = Y_e + (Y_o - Y_e)\sin^2(\Phi/4) \tag{25}$$

$$Y_o(\Phi) = Y(\Phi + 2\pi) = Y_e + (Y_o - Y_e)\cos^2(\Phi/4). \tag{26}$$

Then, from (23)

$$\epsilon_{\text{eff}\,e}(\Phi) = \left[\frac{Y_e + (Y_o - Y_e)\sin^2(\Phi/4)}{Y_{ev} + (Y_{ov} - Y_{ev})\sin^2(\Phi/4)}\right]^2 \tag{27}$$

$$\epsilon_{\text{eff}\,o}(\Phi) = \left[\frac{Y_e + (Y_o - Y_e)\cos^2(\Phi/4)}{Y_{ev} + (Y_{ov} - Y_{ev})\cos^2(\Phi/4)}\right]^2. \tag{28}$$

For the special case of $\Phi = \pi$

$$Y_e(\pi) = Y_o(\pi) \tag{29}$$

$$\epsilon_{\text{eff}\,e}(\pi) = \epsilon_{\text{eff}\,o}(\pi). \tag{30}$$

The above simplification is not possible in the case of $\Phi \neq \pi$.

D. Effective Permeability

Based on the duality of ϵ and μ in the Maxwell's equations, Pucel and Massé [10] derived a relationship between the effective dielectric constant ϵ_{eff} and the effective relative permeability μ_{eff} of a microstrip on a dielectric/mag-

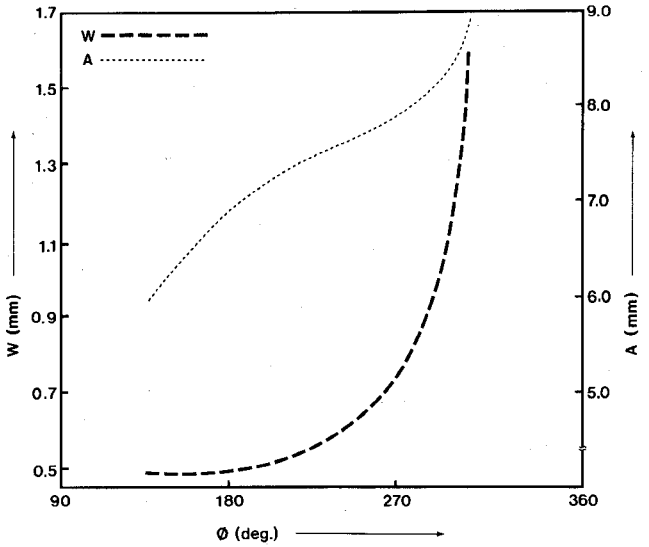

Fig. 5. Variation of the width and the length of the strips of a meanderline for different values of Φ. Impedance level $1/Y_{\text{im}}=50\ \Omega$, spacing $s=0.4$ mm, dielectric constant of the dielectric=2.22.

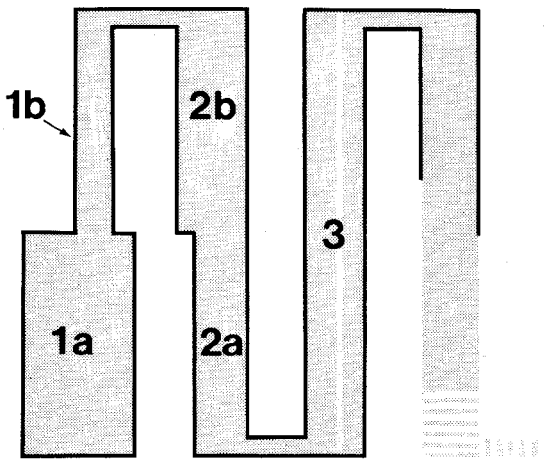

Fig. 6. Stepped admittance design of the meanderline edge sections.

netic substrate. Under similar restrictions, an extension of that relation for the case when two media, dielectric or magnetic, are present, has been derived [15]

$$\mu_{\text{eff}}(\mu_1,\mu_2)=\left[\epsilon_{\text{eff}}\left(\mu_1^{-1},\mu_2^{-1}\right)\right]^{-1}. \tag{31}$$

For gyromagnetic media, expressions given by Massé and Pucel [11] for μ_{dem} and μ_{mag}, corresponding to the demagnetized and "latched" states, are used. Thus the effective relative permeability can also be computed using the filling factors described in the previous subsection.

In summary, for the structure of Fig. 1, the effective dielectric constants are calculated using (27) and (28). The corresponding effective relative permeabilities are given by (31). These results are substituted in (3) to obtain $k_e(\Phi)$ and $k_o(\Phi)$. Then, using $Y_e(\Phi)$ and $Y_o(\Phi)$ calculated from (25) and (26), the length of the meander strips A is computed from (1). Finally, (2) yields Y_{im}, the image admittance of the infinite meanderline structure. To arrive at a particular admittance level one may vary the strip width w while holding the spacing s constant. For an infinite meanderline centered in the four-layer ferrite-dielectric structure of Fig. 1, the widths and the lengths of the strips, obtained for different values of Φ, are shown in Fig. 5. These results are obtained for an impedance level of 50 Ω, a spacing of 0.4 mm between the strips and for a dielectric constant of the dielectric to be 2.22. Beyond $\Phi=270°$, the width and the length of the strips increase rapidly. This is a consequence of the fact that the argument of tangent function on the left-hand side in (1) approaches 90°.

III. Design of Edge Lines

If the coupling between nonadjacent lines is neglected, the edge meander sections can be treated as C-sections. It is known that in microstrip, i.e., in an inhomogeneous environment, a C-section is not well matched [12]. Also, as shown in the case of ferrite microstrip, a C-section designed for a nominal phase difference of $\pi/2$ between the strip centers, is cut off in the vicinity of design frequency [13]. These problems are overcome by adopting the stepped impedance design suggested in [12]. The edge strips are divided into two sections (Fig. 6), with their characteristic admittances given by

$$Y_{ea}\cdot Y_{oa}=(\theta_{ea}/\theta_{oa})\,Y_{\text{im}}{}^2 \tag{32}$$

$$Y_{eb}\cdot Y_{ob}=(\theta_{eb}\tan^2\theta_{ob}/\theta_{ob}\tan^2\theta_{eb})\,Y_{\text{im}}{}^2 \tag{33}$$

where

$$\theta_{ea}+\theta_{oa}=\theta_{eb}+\theta_{ob}=\pi/2. \tag{34}$$

In the above equations, Y_{im} is the matching admittance and the subscripts a and b refer to the corresponding strip sections. In principle, widths of sections $2a$ and $2b$ can be different, but, in practice, the difference is negligibly small.

IV. Synthesis Routine

The synthesis of the phase shifter structure shown in Fig. 1 starts by the calculation of the coefficient matrix $[C]$ given by (5). The concept of filling factors implies that $[C]$ is independent of the material properties. Thus the same coefficient matrix can be used for the optimization of phase shifter structures with different ferrite/dielectric combinations if the geometry is maintained. The effective dielectric constants and the corresponding relative permeabilities are obtained from (27), (28), and (31). The widths of the strips in the meander are then varied until the matching conditions are satisfied. This gives the width and the length of the internal strips. These correspond to a particular spacing between the strips which, for an optimum phase shift, is determined experimentally. Finally, the edge strips are designed according to the method outlined in the previous section.

V. Experimental Results

For the experiments, 0.125-mm-thick RT-Duroid is used as the dielectric. In each case, a 50-Ω meanderline pattern, printed on one of the two dielectric pieces, is sandwiched in a structure similar to the one shown in Fig. 1(a). The

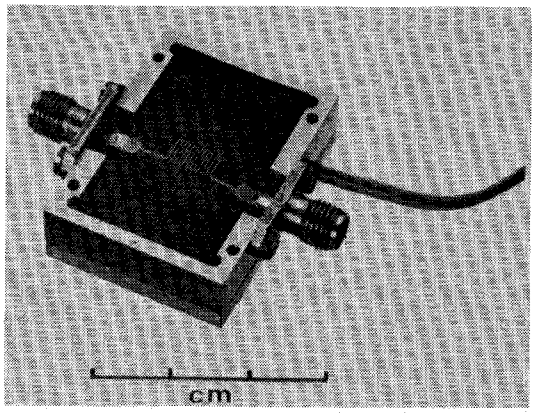

Fig. 7. Phase shifter prototype.

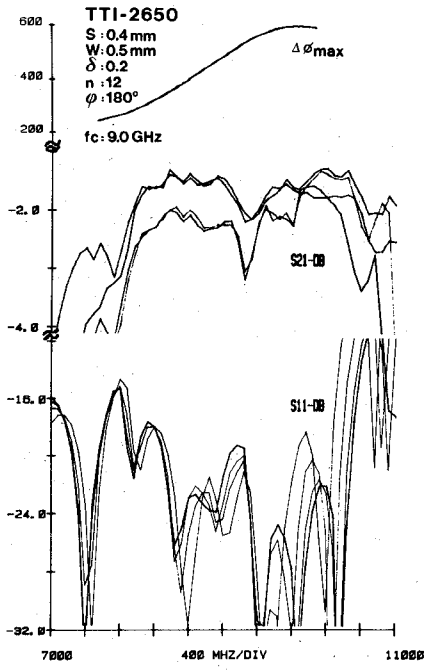

Fig. 8. Maximum differential phase shift, insertion loss, and reflections for different magnetizations, as a function of frequency. Design frequency for the meanderline circuit: 9.0 GHz.

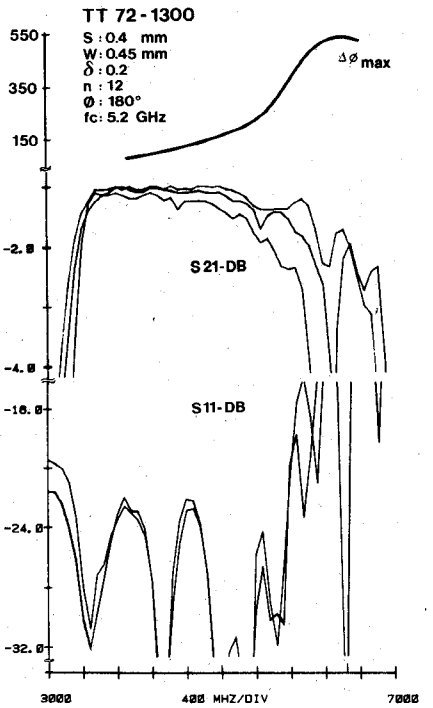

Fig. 9. Same as Fig. 8. Design frequency for the meanderline circuit: 5.2 GHz.

magnetic circuit consists of 1.6-mm-thick ferrite pieces and thin rectangular iron pieces, accurately machined to the required thickness, the latter sitting in slots made in the dielectric pieces. The four-piece toroid so formed is latched to various magnetizations with the help of a magnetizing coil printed on the dielectric piece itself. Trans-Tech ferrites and garnets are used in the experiments. A photograph of the phase shifter is shown in Fig. 7.

Figs. 8 and 9 show the maximum differential phase shift ($\Delta\Phi_{max}$) along with insertion loss and reflections in the case of circuits designed for operation at 9.0 and 5.2 GHz, respectively. In the vicinity of the design frequency the matching is good. While at higher frequencies, the reflections increase sharply due to the approaching stopband of the meander circuit [7]; at lower frequencies, the same occurs due to the rapid change in the impedance of the lines, arising from the frequency dependence of the permeability as ω approaches ω_m [11]. As regards the phase shifts, one can achieve a mean figure of merit of 310°/dB, as seen in the *X*-band case, from 9.4 to 10.0 GHz. On the other hand, there is a considerable variation in phase shift with frequency.

Meanderline circuits represented by Figs. 8 and 9 are designed for $\Phi = 180°$. In these cases, the maximum differential phase shift occurs at a frequency higher than the design frequency. Thus it can be expected that using a somewhat higher value of Φ will bring down the frequency of maximum differential phase shift. Results presented in Fig. 10 verify this. Here, the differential phase shift for a single meander section for three successively higher values of Φ is plotted. For the $\Phi = 260°$ case, allowing for a 5-percent variation in the phase shift, a 16-percent band-

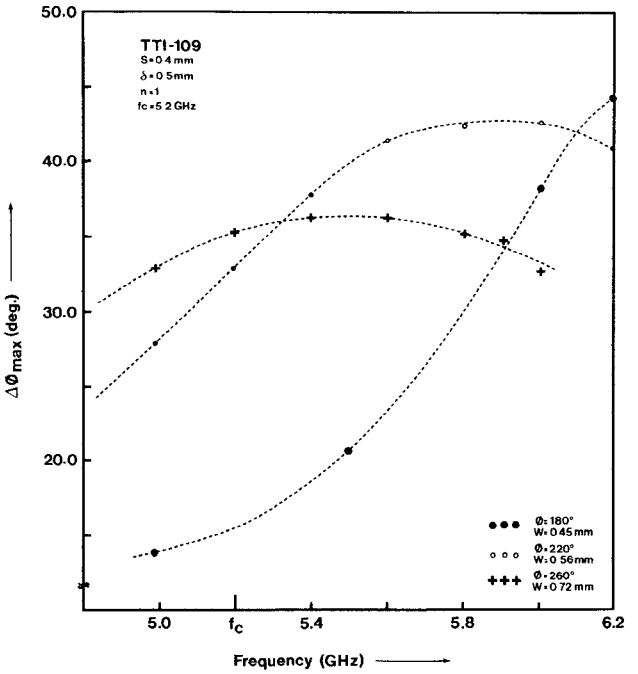

Fig. 10. Maximum differential phase shift versus frequency per single meander section for $\Phi=180°$, 220°, and 260°.

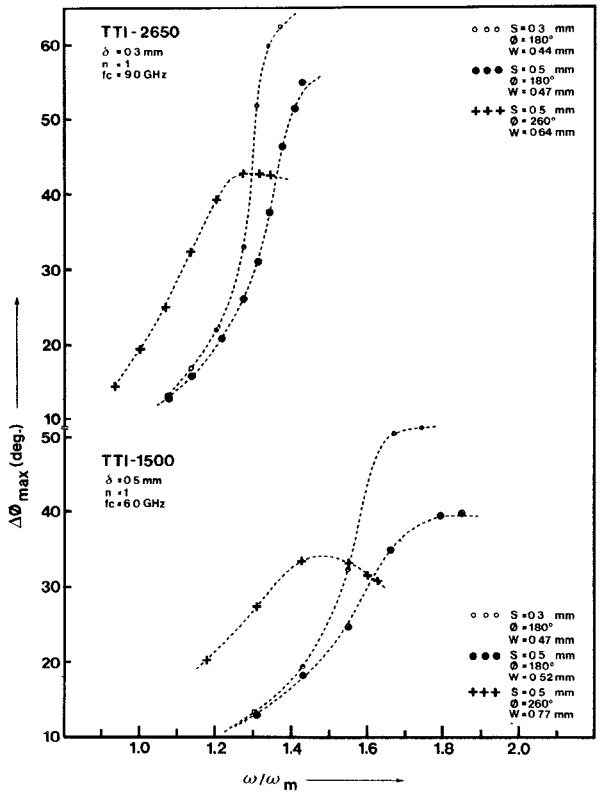

Fig. 11. Maximum differential phase shift per meander section versus frequency, for $\Phi=180°$, for different spacings between the meander strips: $s=0.3$ and $s=0.5$ mm. Also shown are the results for the latter spacing and $\Phi=260°$. For the X-band case, ω/ω_m values are lower.

width is indicated. Therefore, this appears to be an effective way of broad-banding the phase shift. At the same time, however, the available phase shift is lowered. A possible reason for this can be that the ratio s/w is lowered below a certain optimum value. Ongoing experiments indicate that it is possible to improve upon this phase shift value by using a higher impedance level for the meanderline.

Fig. 11 presents the variation in phase shift for different gaps between the adjacent meander strips. Out of the two gap values for which the results are presented, the smaller gap, $s=0.3$ mm, results in a higher maximum differential phase shift. This trend is similar to that for other ferrite phase shifters based on the meanderline circuit, for instance [7]. For the present structure, it is also observed that reflections from the device are higher for $s=0.3$ than for $s=0.5$. This is attributed to the presence of air gaps between the adjacent meander strips, since for a smaller gap these are more difficult to fill in. Also presented in Fig. 10 are the results for $s=0.5$ mm and $\Phi=260°$ for X- and C-band. For these two cases, mean figures of merit of 280°/dB and 250°/dB, respectively, have been achieved. The corresponding bandwidths are approximately 10 and 14 percent.

The peak power threshold, for the parameters given in Fig. 8 ($\omega_m/\omega=0.82$ at 9 GHz), has been measured to be 40 W at 9 GHz and 60 W at 9.3 GHz. It is felt that this threshold could be significantly raised by choosing a lower ω_m/ω [14] or by using a material with a larger spin wave linewidth. The measured values are, however, significantly higher than those expected for a similar structure without the dielectric inserts. Temperature dependence of the phase shift has also been measured in two cases. The results are given in Table I.

TABLE I

Device	Device parameters	Temperature dependence in deg /°C (from -10°C to 60°C)
1.	Material: TTI-2650 Design frequency: 9 GHz	0.5
2.	Material G-1002 Design frequency. 4.5 GHz	0.24

Before concluding this section, it may be mentioned that optimization with respect to the thickness and the dielectric constant of the dielectric, as well as the impedance level of the meanderline, remains to be done.

VI. Conclusions

A method has been given for designing well-matched meanderline circuits for use in planar multilayer ferrite-dielectric phase shifters. Experimental results at C- and X-band have been presented to illustrate the effects of varying different circuit parameters. The results indicate a good figure of merit, which may exceed 300°/dB. For a somewhat lower figure of merit, an operating bandwidth of 10 percent of the design frequency can be easily achieved. This configuration is attractive also for improving peak power threshold and temperature stability.

ACKNOWLEDGMENT

The authors wish to thank Prof. E. F. Bolinder for his encouragement and support. The peak power threshold measurements were done at Telefonaktiebolaget L M Ericsson, Mölndal, Sweden. J. -O. Yxell photo-etched the meanderline patterns, and Miss C. Eliasson typed the manuscript.

REFERENCES

[1] R. R. Jones, "A slow wave digital ferrite strip transmission line phase shifter," *IEEE Trans. Microwave Theory Tech.*, vol. MTT-14, pp. 684–688, Dec. 1966.
[2] J. T. Bolljahn and G. L. Matthaei, "A study of the phase and filter properties of arrays of parallel conductors between ground planes," *Proc. IRE*, vol. 50, pp. 299–311, Mar. 1962.
[3] G. T. Roome and H. A. Hair, "Thin ferrite devices for microwave integrated circuits," *IEEE Trans. Microwave Theory Tech.*, vol. MTT-16, pp. 411–420, July 1968.
[4] C. G. Aumiller, D. H. Harris, M. C. Willson, Y. S. Wu, F. J. Rosenbaum, and D. L. LaCombe, "Ferrite dielectric composite integrated microwave circuit development," in *IEEE G-MTT Int. Microwave Symp. Dig.*, pp. 60–69, 1971.
[5] W. Schilz, "Miniaturized microstrip ferrite phasers," in *Proc. European Microwave Conf.*, vol. 2, paper B. 10.5, 1973.
[6] J. A. Weiss, "Dispersion and field analysis of a microstrip meanderline slow-wave structure," *IEEE Trans. Microwave Theory Tech.*, vol. MTT-22, pp. 1194–1201, Dec. 1974.
[7] F. J. Rosenbaum, "Integrated ferrimagnetic devices," in *Advances in Microwaves*, vol. 8, L. Young and H. Sobol, Eds. New York: Academic Press, 1974, ch.V.
[8] B. Lennartsson, "A network analogue method for computing the TEM characteristics of planar transmission lines," *IEEE Trans. Microwave Theory Tech.*, vol. MTT-20, pp. 586–591, Sept. 1972.
[9] A. Leblond and G. Mourier, "Etude des lignes à barraux à structures periodique pour tubes electronique U.H.F.," *Ann. Radioélect.*, vol. 9, pp. 311–328, 1954.
[10] R. A. Pucel and D. J. Massé, "Microstrip propagation on magnetic substrates—Part I: Design theory," *IEEE Trans. Microwave Theory Tech.*, vol. MTT-20, pp. 304–308, May 1972.
[11] D. J. Massé and R. A. Pucel, "Microstrip propagation on magnetic substrates—Part II: Experiment," *IEEE Trans. Microwave Theory Tech.*, vol. MTT-20, pp. 309–313, May 1972.
[12] B. Schiek and J. Köhler, "A method for broad-band matching of microstrip differential phase shifters," *IEEE Trans. Microwave Theory Tech.*, vol. MTT-25, pp. 666–671, Aug. 1977.
[13] W. M. Libbey, "Characteristics of a microstrip two-meander ferrite phase shifter," *IEEE Trans. Microwave Theory Tech.*, vol. MTT-21, pp. 483–487, July 1973.
[14] W. H. Ince and D. H. Temme, "Phasers and time-delay elements," in *Advances in Microwaves*, vol. 4, L. Young, Ed. New York: Academic Press, 1969, ch. I.
[15] B. Hansson, S. Aditya, and M. Larsson, "Planar meanderline ferrite -dielectric phase shifters," Chalmers University of Technology, Division of Network Theory, Gothenburg, Sweden, Report TR 8004, May 1980.

Printed Circuit Coupled-Line Filters for Bandwidths Up to and Greater than an Octave

BRIAN J. MINNIS

Abstract—**The realization of edge-coupled-line filters as printed circuits has generally been assumed to be confined to filters with fractional bandwidths of 30 percent or less. However, the design technique described herein has eliminated the 30-percent restriction and such filters may now be constructed for fractional bandwidths up to approximately 100 percent. Instead of constraining the physical realization to be a cascade of coupled lines, the technique allows the realization to consist of coupled lines and simple lengths of line cascaded in such a way that resultant circuit dimensions are practicable for the bandwidth specified. Practical examples are described.**

Manuscript received August 6, 1980; revised October 21, 1980.
The author is with Philips Research Laboratories, Redhill, Surrey RH1 5HA, England.

I. INTRODUCTION

THE PRINTED CIRCUIT coupled-line filter consists, in its most familiar form, of a cascade of coupled-line sections all one quarter of a wavelength long at a common

0018-9480/81/0300-0215$00.75